The shadows of accelerating Kerr-Newman black hole and constraints from M87*

Tao-Tao Sui [a,*], Qi-Ming Fu [b,c], Wen-Di Guo [d]

[a] *College of Physics, Nanjing University of Aeronautics and Astronautics, Nanjing 211106, China*
[b] *Institute of Physics, Shaanxi University of Technology, Hanzhong 723000, China*
[c] *Department of Physics, College of Sciences, Northeastern University, Shenyang 110819, China*
[d] *Institute of Theoretical Physics & Research Center of Gravitation, Lanzhou University, Lanzhou 730000, China*

ARTICLE INFO

ABSTRACT

In this paper, we study the influence of the parameters for the accelerating Kerr-Newman black hole on the shadows and the constraints, extensively. We find that the rotating parameter a, the charge parameter e, and the inclination angle θ_0 affect the shadow qualitatively similar to that of Kerr-Newman black holes. The result shows that the size of the shadow will scale down with the accelerating factor A. Besides, the factor A also can affect the best viewing angles, which make the observations maximum deviate from $\theta_0 = \frac{\pi}{2}$, and the degree of the deviations are less than 1%. Then, we assume the M87* as an accelerating Kerr-Newman black hole with the mass $M = 6.5 \times 10^9 M_\odot$ and the distance $r_0 = 16.8 Mpc$. Combining the EHT observations, we find that neither the observations, circularity deviation ΔC or axial ratio D_x can distinguish the accelerating black hole or not. However, the characteristic areal-radius of the shadow curve R_a can give corresponding constraints on the parameters of the accelerating Kerr-Newman black hole. The result shows that the bigger accelerating factor A is, the stronger constraints on the rotating parameter a and charged parameter e. The maximum range of the accelerating factor is $A r_0 \leq 0.558$ for a accelerating Schwarzschild case with $(a/M = e/M = 0)$, and for an extremely slow accelerating case $(A r_0 \leq 0.01)$, the ranges of rotating parameter a and charged parameter e are $a/M \in (0, 1)$ and $e/M \in (0, 0.9)$.

1. Introduction

When the photons move around a black hole, they will face three kinds of destinies, i.e., absorbed by the black hole, reflected by the black hole, or revolving around the black hole. For the third destiny, the photons are trapped in unstable circular geodesics, defining the photon sphere. The photon sphere can describe the outline of the black hole, also named with the shadow of the black hole. Besides, perturbations within the photon sphere give rise to the familiar excitations known as photon sphere quasinormal modes [1,2].

In the 1960s, Synge calculated the shadow of a spherically symmetric Schwarzschild black hole [3]. Then, Luminet considered the case that the Schwarzschild black hole surrounded by an accretion disk, and calculated the size of the shadow [4]. In Ref. [5], the authors studied the shadow of a rotating black hole, and the result shows that with the dragging effect of rotation, the shadow will

deviate from the perfect circle. Then, the study on the shadow of different spacetime geometries has been blooming with the motivation that the non-circular shadow, including black hole [6–22], and wormhole [23–30].

More recently, the Event Horizon Telescope (EHT) Collaboration gave the image of the supermassive black hole M87*, which is the first image of the shadow for the black hole and makes the theoretical prophecy of the black hole shadow become physical reality [31–36]. The shadow of M87* gives the observations with the derivation circularity $\Delta C \lesssim 0.1$, the axis ratio $1 < D_x \lesssim 4/3$, and the angular shadow diameter $\psi_d = 3\sqrt{3}(1 \pm 0.17)\psi_g$, with the angular gravitational radius $\psi_g = 3.8 \pm 0.4 \mu as$. Combining with these observations of M87*, the authors have effectively constrained the characteristics of Kerr-like black holes [37–39]. Furthermore, various methods exist for constraining black hole properties. For instance, Kuang and Ali employ gravitational lensing to constrain Kerr-like black holes [40], while Destounis et al. establish limitations for non-Kerr black holes [41–44] as well as exotic compact objects [45,46] through gravitational-wave observables. Addition-

* Corresponding author.
E-mail addresses: suitt14@lzu.edu.cn (T.-T. Sui), guowd@lzu.edu.cn (W.-D. Guo).

ally, there are endeavors to constrain non-vacuum black holes situated within astrophysical contexts [47–50].

According to previous works, we can find that many rotating black boles share a similar characteristic, that the inclination angle of the observer equals $\pi/2$, which makes the observations of the shadows for these black holes maximum. Besides, all these researches show that the apparent characteristics of the black hole shadows vary with the parameters of the black holes, which are closely connected with the essential properties of gravity theory and the background fields. In other words, the different characteristics of black hole shadows can reflect the different forms of black hole solutions.

On the other hand, there is a special family of black hole solutions in the Einstein's general relativity named as C-metric [51–55], which can describe the accelerating black hole and belongs to the well-known Plebański-Demiański spacetime [56,57]. Many works not only focus on the thermodynamics of the C-metric [58–61], but also on its stability, superradiance effect and the validity of strong cosmic censorship in these spacetimes [62–65]. In Refs. [66,67], the authors just analyzed the shadows of the accelerating Kerr black holes theoretically. The result shows that the acceleration of the black hole has an unique influence on the properties of the shadow.

In Ref. [68], the authors obtained the consistent thermodynamic description of the accelerating charged and rotating black hole, which also can be named as accelerating Kerr-Newman (KN) black hole. Inspired by the previous works [66,67], we can not only investigate the influence of the parameters, i.e. the rotating parameter, the charged parameter, and the accelerating parameter on the shadow for the accelerating KN black hole, and analyze the characterized observables of the black bole shadow, theoretically. But also, we can consider the supermassive black hole M87* as the accelerating KN black hole and constrain the corresponding parameters with the EHT observations.

The main parts of this paper are organized as follows. In Sec. 2, we will investigate the circular orbits of the photons around the accelerating Kerr-Newman black hole. In Sec. 3, we will consider the influence of the parameters on the shadow for the accelerating Kerr-Newman black hole. We presuppose the M87* as the accelerating Kerr-Newman black hole, and get the constraints of the corresponding parameters from the EHT observations in Sec. 4. The last section contributes to our closing summary.

2. Circular photon orbits around the accelerating Kerr-Newman black hole

In this section, we first give a brief review of the accelerating KN black hole, the line element can be described as [68]

$$ds^2 = \frac{1}{H^2}\left\{ -\frac{\Delta_r}{\Sigma}\left(\frac{dt}{\alpha} - a\sin^2\theta d\phi\right)^2 + \frac{\Sigma}{\Delta_r}dr^2 + \frac{\Sigma}{\Delta_\theta}d\theta^2 \right.$$
$$\left. + \frac{\Delta_\theta}{\Sigma}\left(\frac{adt}{\alpha} - (r^2+a^2)d\phi\right)^2 \right\}, \tag{1}$$

with

$$H = 1 + Ar\cos\theta, \ \Sigma = r^2 + a^2\cos^2\theta,$$
$$\Delta_r = (1 - A^2 r^2)(r^2 - 2Mr + a^2 + e^2),$$
$$\Delta_\theta = 1 + 2MA\cos\theta + A^2(a^2 + e^2)\cos^2\theta, \tag{2}$$
$$\alpha = \frac{\sqrt{(1 - a^2 A^2)(1 + a^2 A^2 + e^2 A^2)}}{1 + a^2 A^2},$$

and the corresponding gauge potential can be expressed as

$$F = dB,$$
$$B = -\frac{e}{\Sigma r}\left(\frac{dt}{\alpha} - a\sin^2\theta d\phi\right) + \frac{er_+}{(a^2 + r_+^2)\alpha}dt, \tag{3}$$

where r_+ is the radius of the event horizon of the accelerating KN black hole with $\Delta_r(r_+) = 0$.

In the charged accelerating Kerr black hole, the parameters m, a and e are the mass, rotation and charge parameters, respectively. The parameter A represents the acceleration factor of the black hole. H is the conformal factor, which can affect the conformal boundary r_B of the accelerating black hole with $r_B = \frac{1}{|A\cos\theta|}$. The parameter α can rescale the time coordinate and ensure the Killing vector be normalized at conformal infinity. The term Δ_r can also be expressed as $\Delta_r = (r - r_-)(r - r_+)(r^2 - r_A^2)$, where $r_\pm$ are identical to the event and Cauchy horizons of the non-accelerating KN black hole, $r_A = 1/A$ is already familiar in the context of the C-metric as an acceleration horizon. With the conformal boundary r_B, the range of r should be constrained as $r_+ \leq r \leq r_B$. Besides, in order to make sure that the accelerating KN black hole in the bulk, the term $\Delta_r = 0$ should have roots in the range $r < r_A$ [68].

Then, the Lagrange for the photons can be described by

$$\mathcal{L} = \frac{1}{2}g^{\mu\nu}\dot{x}_\mu \dot{x}_\nu, \tag{4}$$

with the definition $\dot{x}^\mu = dx^\mu/d\lambda = u^\mu$, where u^μ is the four-velocity of the photon and the parameter λ is the affine parameter. For this stationary black hole, there are two Killing vectors ∂_t and ∂_ϕ which can result the conserved total energy E and z-component of the angular momentum L_z.

Using the Hamilton-Jacobi equation, we can get the null geodesic equation of the photon on the background of the accelerating KN black hole

$$\frac{\Sigma}{H^2}\frac{dt}{d\lambda} = \frac{\alpha\left(a^2 + r^2\right)\left(\alpha E\left(a^2 + r^2\right) - aL_z\right)}{\Delta_r}$$
$$+ \frac{a\alpha\left(L_z - a\alpha E\sin^2\theta\right)}{\Delta_\theta}, \tag{5}$$

$$\frac{\Sigma}{H^2}\frac{d\phi}{d\lambda} = \frac{a\left(\alpha E\left(a^2 + r^2\right) - aL_z\right)}{\Delta_r}$$
$$+ \frac{\left(L_z\csc^2\theta - a\alpha E\right)}{\Delta_\theta}, \tag{6}$$

$$\left(\frac{\Sigma}{H^2}\right)^2\left(\frac{dr}{d\lambda}\right)^2 = \left[(a^2 + r^2)E - aL_z\right]^2 - \Delta_r Q \equiv R(r), \tag{7}$$

$$\left(\frac{\Sigma}{H^2}\right)^2\left(\frac{d\theta}{d\lambda}\right)^2 = \Delta_\theta Q - \frac{(L_z - aE\sin^2\theta)^2}{\sin^2\theta} \equiv \Theta(\theta), \tag{8}$$

where parameter Q is the Carter constant [69] and the functions $R(r)$ and $\Theta(\theta)$ can be considered as the radial and longitudinal effective potential, respectively.

Since the photon orbits should independent of the energy, we can introduce the following dimensionless abbreviations to describe the photon orbits

$$\xi = \frac{L_z}{E}, \quad \eta = \frac{Q}{E^2}. \tag{9}$$

Generally, the unstable spherical circular photon orbits should satisfy with the conditions

$$R(r) = 0, \quad \frac{dR(r)}{dr} = 0. \tag{10}$$

According to the above two conditions, the dimensionless quantities ξ, and η can be solved as

$$\xi = \frac{a^2 \partial_r \Delta_r + r^2 \partial_r \Delta_r - 4r\Delta_r}{a \, \partial_r \Delta_r}, \tag{11}$$

$$\eta = \frac{16 r^2 \Delta_r}{(\partial_r \Delta_r)^2}. \tag{12}$$

By plugging these expressions into Eq. (8), we can find that the non-negativity of Eq. (8) gives the condition for the photon region as

$$(4r\Delta_r - \Sigma \partial_r \Delta_r)^2 \le 16 a^2 r^2 \Delta_r \Delta_\theta \sin^2 \theta. \tag{13}$$

For the non-rotating case $a = 0$, the circular orbit radius can be solved from the unstable spherical circular photon orbits conditions (10) as

$$r_p = \frac{-1 + A^2 e^2}{3A^2 M} + 2\sqrt{\beta} \cos\left[\frac{1}{3}\cos^{-1}(\alpha\beta^{-\frac{3}{2}})\right], \tag{14}$$

with

$$\alpha = \frac{2\left(A^2 e^2 - 1\right)^3 - 27 A^2 M^2 \left(A^2 e^2 + 1\right)}{54 A^6 M^3},$$

$$\beta = \frac{1}{A^2} + \frac{\left(A^2 e^2 - 1\right)^2}{9 A^4 M^2}. \tag{15}$$

3. The shadows of the charged accelerating Kerr black holes

For calculating the character of the black hole shadow, which can be seen by an observer, we should assume a normalized and orthogonal frame where the observer is located at, and this frame can be expressed as following

$$\hat{e}_{(t)} = \sqrt{\frac{g_{\phi\phi}}{g_{t\phi}^2 - g_{tt} g_{\phi\phi}}} \left(\partial_t - \frac{g_{t\phi}}{g_{\phi\phi}} \partial_\phi\right), \tag{16}$$

$$\hat{e}_{(r)} = \frac{1}{\sqrt{g_{rr}}} \partial_r, \ \hat{e}_{(\theta)} = \frac{1}{\sqrt{g_{\theta\theta}}} \partial_\theta, \ \hat{e}_{(\phi)} = \frac{1}{\sqrt{g_{\phi\phi}}} \partial_\phi. \tag{17}$$

In this frame, we can see that the observer is locally static and zero angular momentum with respect to infinity for $\hat{e}_{(t)} \cdot \partial_\phi = 0$. Hence, this frame also can be named as zero-angular-momentum-observer (ZAMO) reference frame.

For describing the shadow of the accelerating KN black hole, we should project the 4-momentum p^μ of photon onto the ZAMO reference frame where the observer located at, and the corresponding quantities measured by the observer can be expressed as

$$p^{(t)} = -p_\mu \hat{e}_{(t)}^\mu, \quad p^{(i)} = p_\mu \hat{e}_{(i)}^\mu, \ i = r, \theta, \phi. \tag{18}$$

In the ZAMO frame, the spatial component of momentum $|\vec{P}|$ should satisfy $|\vec{P}| = p^{(t)}$ for the massless photon. In order to express the specific 3-momentum p^i, we can introduce the observation angles (α, β) as [70]

$$p^{(r)} = |\vec{P}| \cos\alpha \cos\beta, \ p^{(\theta)} = |\vec{P}| \sin\alpha,$$

$$p^{(\phi)} = |\vec{P}| \cos\alpha \sin\beta. \tag{19}$$

Combining the geodesic equations (5)-(8) together, we can obtain

$$\sin\alpha = \frac{p^{(\theta)}}{p^{(t)}} = \pm \frac{H}{\zeta - \gamma\xi}$$

$$\times \sqrt{\frac{\eta}{\Sigma} - \frac{(a\sin^2\theta - \xi)^2}{\Sigma \Delta_\theta \sin^2\theta}}\Big|_{(r_O, \theta_O)}, \tag{20}$$

$$\tan\beta = \frac{p^{(\phi)}}{p^{(r)}} = \frac{\xi\sqrt{\Sigma\Delta_r}}{H\sqrt{g_{\phi\phi}}}$$

$$\times \left[(r^2 + a^2 - a\xi)^2 - \Delta_r \eta\right]^{-\frac{1}{2}}\Big|_{(r_O, \theta_O)}. \tag{21}$$
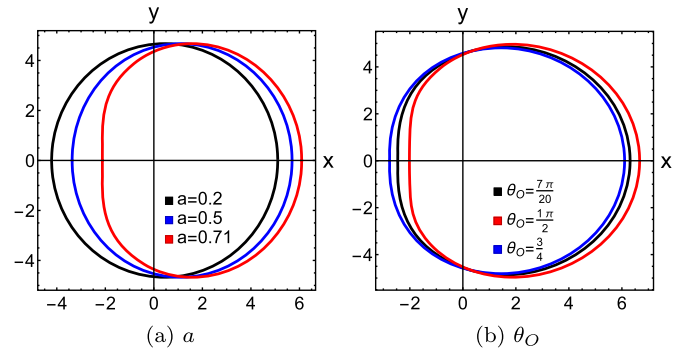

Fig. 1. The examples of shadows for the accelerating KN black holes with different parameters. The other parameters are set as $\theta_O = \frac{\pi}{2}, e = 0.4, A = 0.002$ for (a) and $e = 0.4, a = 0.9, A = 0.002$ for (b).

Here, to simplify the above expression, we set the abbreviations $\zeta \equiv \hat{e}_{(t)}^t$, and $\gamma \equiv \hat{e}_{(t)}^\phi$. The parameters r_O and θ_O are the radial position and the inclination angle between the observer and the direction of the rotation axis for the black hole.

3.1. The shadows

Furthermore, in order to obtain the apparent position on the plane of the sky for the observer, we need to introduce the Cartesian coordinate (x, y) as

$$x \equiv -r_O \beta, \quad y \equiv r_O \alpha. \tag{22}$$

We can see that both the coordinates x and y are the functions of (r_0, θ_O, a, e, A). We show the shadows of the accelerating KN black hole for the variables a, e, A and θ_O in Figs. 1 and 2, where we set $M = 1$ and $r_O = 100$. From Fig. 1(a), we can see that with the increasing of the angular momentum a, the shape of the rotating black hole shadow becomes non-circular as the result due to the dragging effect. Besides, Fig. 1(b) shows that the observable dragging effect which can result in the shadows of rotating black hole deviating from the standard circle also depends on the observation angle θ_O, even though the charged accelerating Kerr black hole with large rotating parameter. From Fig. 2, we should note that the size of the black hole shadow decreases with the charge parameter e and the acceleration factor A. At the same time, as the charge parameter e increases, the non-circular behavior of black hole shadows becomes more significant. Summing up, we can draw a conclusion that the phenomena for the shadow of Kerr black hole deviating from the standard circle are mainly caused by the rotating of the black hole, and the presence of charge of the black hole will assist in the generation of the phenomena, which is similar to that of the Kerr-Newman cases [71–74]. Furthermore, the acceleration factor A can have an effect on the size of the shadow for the black hole, and we will further investigate other influences of the factor A on the shadow in the next part.

3.2. The observables

In the previous section, we analyzed the influence of the parameters for the accelerating KN black holes on their shadows. However, we only can get the shadows of the black hole by astronomical observation. So, in order to know the characters of the accelerating KN hole by the astronomical observed data, we should construct some easily measured and reliable astronomical observables. Here, we will consider the following observables with the radius R_s and the distortion parameter δ_s, which are defined by Hioki and Maeda [75]. The parameter R_s can be considered as a radius of the reference circle which should pass the top point
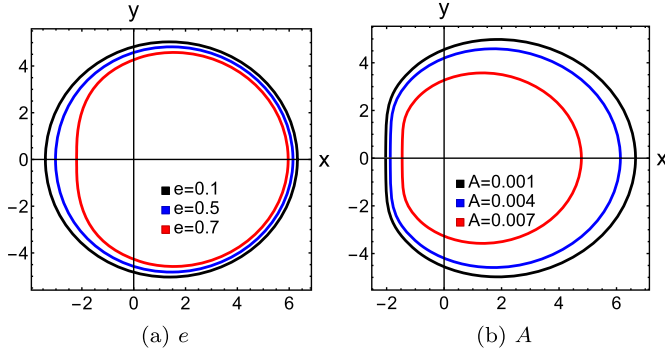
(a) e (b) A

Fig. 2. The patterns of shadows of the accelerating KN black holes with different parameters. The other parameters are set as $\theta_O = \frac{\pi}{2}, a = 0.7, A = 0.002$ for (a) and $\theta_O = \frac{\pi}{2}, a = 0.7, e = 0.7$ for (b).

(x_t, y_t), the bottom point (x_b, y_b), and the right point $(x_r, 0)$ of the shadow, and the distortion parameter δ_s can measure the distortion of the black hole shadow compared with the reference circle, which can be defined as

$$R_s = \frac{(x_t - x_r)^2 + y_t^2}{2(x_r - x_t)}, \quad \delta_s = \frac{x_l - \tilde{x}_l}{R_s}, \tag{23}$$

where $(x_l, 0)$ and $(\tilde{x}_l, 0)$ are the left points of the shadow and reference circle, respectively.

Fig. 3 displays the influence of the rotation parameter a and charge parameter e on the observable parameters R_s and δ_s. From Fig. 3(a), we can see that the radius parameter R_s decreases rapidly with the increasing charge parameter e. While, the rotating parameter a slightly affect the reference circle R_s. For the distortion parameter δ_s, Fig. 3(b) shows that the distortion of the shadow for the accelerating KN black hole increases with the rotation parameter a, and the effect of charged parameter e is slight. The effects of the rotating parameter a and the charged parameter e on the astronomical observables R_s and δ_s, are similar to that of Kerr-Newman black hole [21].

In previous chapter, the result shows that the acceleration factor A can affect the size of the shadow of the black hole, which can also be verified in Fig. 4(a). From Fig. 4, we can see that the observation angle θ_O results a slighter influence on the radius R_s, but a larger effect on the distortion δ_s. Furthermore, when the inclination angle $\theta_0 \approx \frac{\pi}{2}$, both R_s and δ_s reach the maximum value, with other parameters are fixed.

In order to ascertain the influence of the acceleration factor A on the best viewing angle θ_0 which makes the radius R_s or δs maximum, we can introduce the deviation angle θ_R and θ_s with the definition as [67]

$$\theta_R = \frac{\pi}{2} - \theta_b|_{(R_s = R_{max})}, \tag{24}$$

$$\theta s = \frac{\pi}{2} - \theta_b|_{(\delta s = \delta_{smax})}. \tag{25}$$

Fig. 5 shows the variation of the degree of deviation angles θ_R and θ_s as the result of the accelerating factor A. For the deviation angle θ_R, Fig. 5(a) shows that the deviation angle θ_R decreases with the charged parameter e, while the rotating parameter a has no effect on θ_R. From Fig. 5(b), we can see that the deviation angle θ_s decreases with both the rotating parameter a and charged parameter e. Besides, both the deviation angles θ_R and θ_s increase with the accelerating factor A. While, the accelerating factor A has a greater influence on the deviation angle θ_R than on θ_s, and the degree of the deviations are less than 1%.
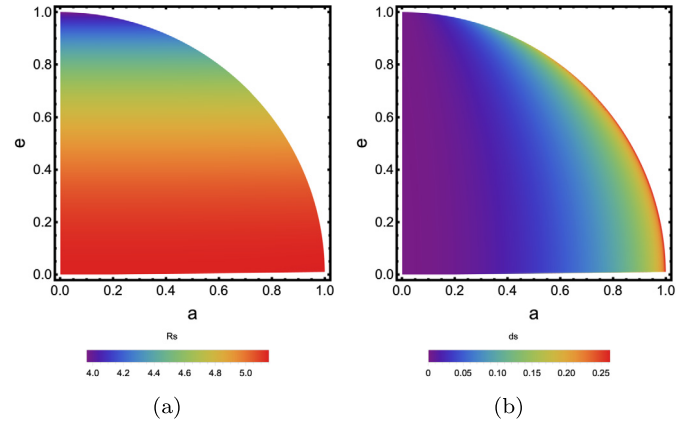

(a)   (b)

Fig. 3. The density plots of the observable parameters R_s and δs with the variables (a, e). The other parameters are set as $\theta_O = \frac{\pi}{2}, r_0 = 100$, and $A = 0.005$.
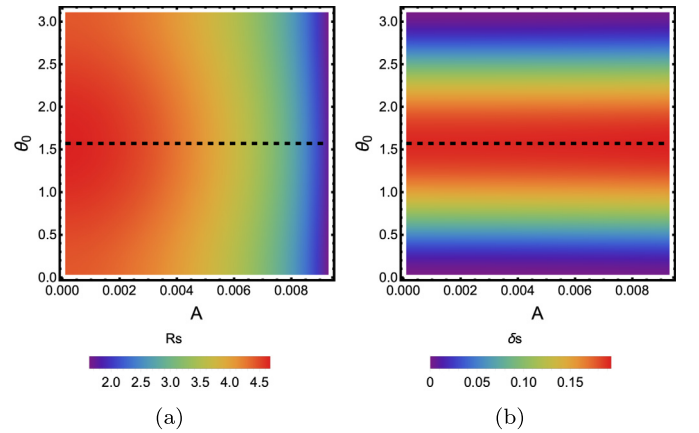

(a)   (b)

Fig. 4. The density plots of the observable parameters R_s and δs with the variables (A, θ_0). Here, the other parameters are set as $r_0 = 100$, $a = 0.7$, and $e = 0.7$. The dashed black lines denote R_s and δs with $\theta_0 = \frac{\pi}{2}$.

4. Constraints of the parameters from M87*

The shadow image of the supermassive black hole M87* as crescent shaped was photographed by the EHT collaboration with the mass $M = 6.5 \times 10^9 M_\odot$, the distance $r_0 = 16.8 Mpc$, and the inclination angle $\theta_0 = 17^o$ [31–36]. The preliminary analysis of the EHT observations constrain the root-mean-square distance from the average radius of the black hole shadow as $\Delta C \lesssim 0.1$ which also named as circularity deviation, the axis ratio as $1 < D_x \lesssim 4/3$. Then, in Refs. [76,77], the authors addressed that the shadow size of M87* should lie in the range as $R_a \approx 3\sqrt{3}(1 \pm 0.17)M$. Many works have used these shadow observables ΔC, D_x and R_a to constrain the parameters of corresponding black holes [78–80]. Inspired by these works, we consider the accelerating charged rotating black hole as the supermassive black hole in M87*, and use the EHT observations to give the constraints on the corresponding parameters.
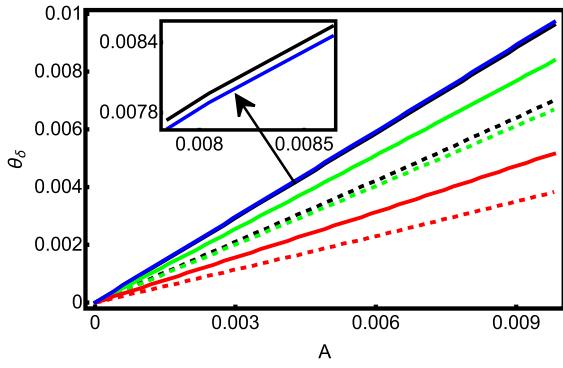
To obtain the constraints, we should introduce the explicit definitions of the observables ΔC, D_x and ψ_d, respectively. The center of the shadow can be set as $(x_c = \frac{x_r + x_l}{2}, y_c = 0)$. The boundary of the shadow can be expressed with the polar coordinates $(\phi, R(\phi))$ as

$$\phi = \tan^{-1}\left(\frac{y}{x - x_c}\right), \quad R(\phi) = \sqrt{(x - x_c)^2 + y^2}, \tag{26}$$

and the circularity deviation ΔC of the black hole shadow can be defined as [79]
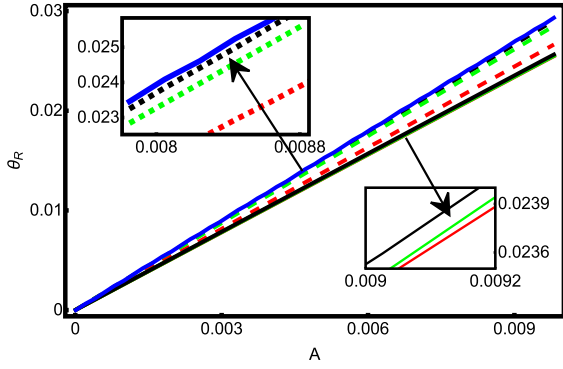
(a)

(b)

Fig. 5. The diagrams for the deviation of the inclination angle which makes the shadows radius R_s and the distortion δ_s maximum. Here, we set $M = 1$ and $r_0 = 100$. The dashed lines are black ($e = 0.2$), green ($e = 0.4$), and red ($e = 0.59$) with $a = 0.8$. The solid lines are black ($a = 0.2$), green ($a = 0.4$), and red ($a = 0.7$) with $e = 0.7$. Besides, the solid blue line is ($a = 0.05, e = 0$).

$$\Delta C = \frac{1}{\bar{R}} \sqrt{\int_0^{2\pi} (R(\phi) - \bar{R})^2 d\phi}, \tag{27}$$

with the average radius

$$\bar{R} = \frac{1}{2\pi} \int_0^{2\pi} R(\phi) d\phi. \tag{28}$$

The axis ratio is expressed [81,82]

$$D_x = \frac{y_t - y_b}{x_r - x_l}, \tag{29}$$

and the definition of the characteristic areal radius of the shadow curve can be expressed as [82,83]

$$R_a = \sqrt{\frac{2}{\pi} \int_{r_{min}}^{r_{max}} \left(y(r) \frac{dx(r)}{dr} \right)}. \tag{30}$$

From the definitions of the observations, we can see that both the circularity deviation ΔC and the axis ratio D_x are the relative observations, which means the expansion or reduction of the outline for the shadow will not affect ΔC or D_x. Roughly speaking, Fig. 2(b) shows that with the accelerating factor A increasing, the diagrams of the shadow for the accelerating KN black hole will scale down, which implies that the EHT observables ΔC, D_x might not impose limitations on the range of accelerating factor A. This conclusion gains further support from Fig. 6, which confirms that
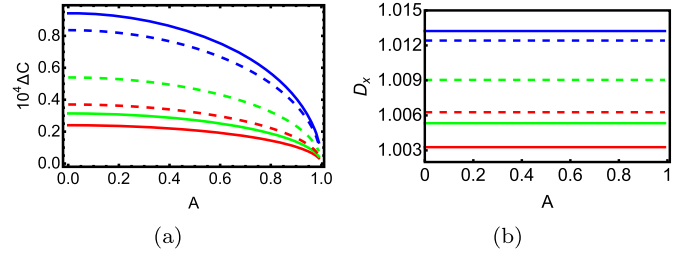

(a)

(b)

Fig. 6. The density diagrams of the circularity ΔC and axial ratio D_x with the ETH data $M = 6.5 \times 10^9 M_\odot$, $r_0 = 16.8 Mpc$, and $\theta_0 = 17^o$. The solid lines are red ($a = 0.6$), green ($a = 0.7$), and blue ($a = 0.86$) with $e = 0.5$. The dashed lines are red ($e = 0.3$), green ($e = 0.5$) and green ($e = 0.76$) with $a = 0.8$.
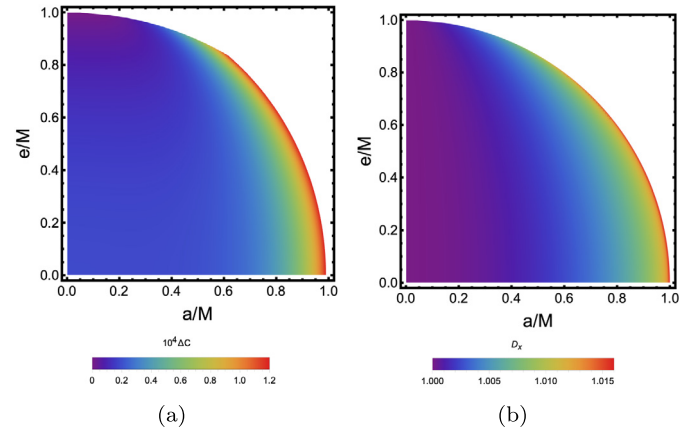

(a)

(b)

Fig. 7. The density diagrams of the circularity ΔC and axial ratio D_x in the (a, e) plane with the ETH data $M = 6.5 \times 10^9 M_\odot$, $r_0 = 16.8 Mpc$, and $\theta_0 = 17^o$. The parameter A is set as $A = 0.01 \frac{1}{r_0}$.

the EHT observations $\Delta C \lesssim 0.1$ and $D_x \lesssim 4/3$ are insufficient to effectively constrain the accelerating factor A. Additionally, Fig. 6 reveals a diminishing trend in circularity deviation ΔC with increasing accelerating factor A, while the impact of accelerating factor A on the axis ratio D_x remains negligible. Furthermore, for a KN black hole with near-extreme behavior or large rotation parameter a, both ΔC and D_x are more pronounced. Consequently, to establish constraints on the parameters of the accelerating KN black hole using the EHT observables ΔC and D_x, it is advisable to present the outcomes in the (a, e) plane. From Fig. 7, we can see that the whole parameters space of (a, e) satisfy the EHT observations $\Delta C \lesssim 0.1$ and $D_x \lesssim 4/3$, which indicates that it is impossible to make any constraint on the parameters of the accelerating KN black hole.

Fig. 8 shows the constraints of the parameters for the black hole by the EHT observation with the shadow size R_a. All the real curves represent the lower bound $R_a = 4.31M$, and the reasonable parameters with the constraints below these curves. The results illustrate that the bigger accelerating factor A, the stronger restriction on the rotating parameter a and charge parameter e. From the extremely slow accelerating case, i.e., $Ar_0 \leq 0.01$, the charge parameter e has maximum range as $e/M \in (0, 0.9)$, which is consistent with the conclusion in [77]. While, according to the range of shadow size R_a, we can not make any constraints on the rotating parameter a. Furthermore, we consider the maximum value range of the accelerating factor A by setting the parameters as $a/M = e/M = 0$ and the result shows that $Ar_0 \in (0, 0.558)$, which is shown in Fig. 9.
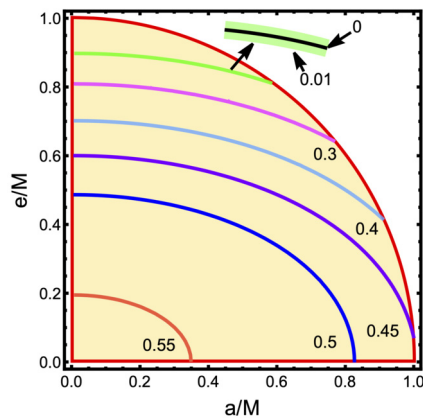
Fig. 8. The constraints of the ETH observation $4.31M \leq R_a \leq 6.08M$ on the parameters (a, e). The real curves represent $R_a = 4.31M$ with different accelerating factor A.
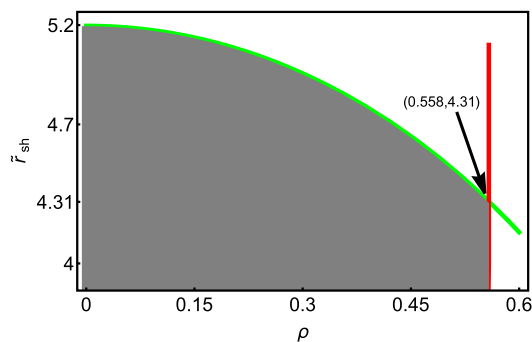

Fig. 9. The constraint of the ETH observation $4.31M \leq R_a \leq 6.08M$ on the accelerating factor A with the parameters $a/M = e/M = 0$.

5. Summary

In this paper, we concentrated on the shadow of the accelerating KN black hole, and analyzed the influence of the parameters on the shadow and its observables. The rotating parameter a, the charged parameter e, and the inclination angle θ_0 affect the shadow with the qualitatively similar to that of Kerr-Newman black holes [37,71–74]. Besides, the size of the shadow for the accelerating KN black hole case will scale down with the accelerating factor A.

Then, we analyzed the influence of the parameters on the shadow observables, i.e., the reference radius R_s and the distortion δs. The rotating parameter a dominates the change of the distortion δs, and the reference radius R_s decreases with the charge parameter e, rapidly. The result shows that although the accelerating factor A can affect the best viewing angle, which makes R_s or δs maximum, the deviations from $\theta_0 = \frac{\pi}{2}$ are limited, i.e., the deviations are less than 1%.

Finally, we assumed the accelerating KN black hole as the supermassive M87* black hole, and used the EHT observables to constrain the black hole parameters. We found that the whole parameters space (a, e) satisfy the EHT observables ΔC and D_x constraints, which means that it can not rule out the supermassive M87* black hole is an accelerating KN black hole through the EHT observables ΔC and D_x. On the other hand, according to the observable shadow size R_a, the result shows that the bigger accelerating factor A is, the smaller ranges of parameter a and e are. For an extremely slow accelerating case ($Ar_0 \leq 0.01$), the ranges of rotating parameter a and charge parameter e are $a/M \in (0, 1)$ and $e/M \in (0, 0.9)$. The maximum range of the accel-

erating factor is $Ar_0 \leq 0.558$ for a accelerating Schwarzschild case with $(a/M = e/M = 0)$.

Declaration of competing interest

The authors declare that they have no known competing financial interests or personal relationships that could have appeared to influence the work reported in this paper.

Data availability

No data was used for the research described in the article.

Acknowledgements

References

[1] V. Cardoso, A.S. Miranda, E. Berti, H. Witek, V.T. Zanchin, Geodesic stability, Lyapunov exponents and quasinormal modes, Phys. Rev. D 79 (2009) 064016, arXiv:0812.1806.

[2] V. Cardoso, J.L. Costa, K. Destounis, P. Hintz, A. Jansen, Quasinormal modes and strong cosmic censorship, Phys. Rev. Lett. 120 (2001) 031103, arXiv:1711.10502.

[3] J.L. Synge, The escape of photons from gravitationally intense stars, Mon. Not. R. Astron. Soc. 131 (1966) 463.

[4] J.-P. Luminet, Image of a spherical black hole with thin accretion disk, Astron. Astrophys. 75 (1979) 228.

[5] J.M. Bardeen, et al., Les Houches Summer School of Theoretical Physics: Black Holes, Gordon and Breach Science Publishers, Inc., United States, 1973, pp. 215–240.

[6] K. Hioki, U. Miyamoto, Hidden symmetries, null geodesics, and photon capture in the Sen black hole, Phys. Rev. D 78 (2008) 044007, arXiv:0805.3146.

[7] A. Grenzebach, V. Perlick, C. Lämmerzahl, Photon regions and shadows of Kerr-Newman-NUT black holes with a cosmological constant, Phys. Rev. D 89 (2014) 124004, arXiv:1403.5234.

[8] M.-Z. Wang, S.-B. Chen, J.-J. Jing, Shadows of Bonnor black dihole by chaotic lensing, Phys. Rev. D 97 (2018) 064029, arXiv:1710.07172.

[9] M. Guo, N.A. Obers, H. Yan, Observational signatures of near-extremal Kerr-like black holes in a modified gravity theory at the Event Horizon Telescope, Phys. Rev. D 98 (2018) 084063, arXiv:1806.05249.

[10] P.-C. Li, M. Guo, B. Chen, Shadow of a spinning black hole in an expanding Universe, Phys. Rev. D 101 (2020) 084041, arXiv:2001.04231.

[11] H.-P. Yan, Influence of a plasma on the observational signature of a high-spin Kerr black hole, Phys. Rev. D 99 (2019) 084050, arXiv:1903.04382.

[12] R.A. Hennigar, M.B.J. Poshteh, R.B. Mann, Phys. Rev. D 97 (2018) 064041, arXiv:1801.03223.

[13] R. Konoplya, Shadow of a black hole surrounded by dark matter, Phys. Lett. B 795 (2019) 1, arXiv:1905.00064.

[14] C. Bambi, K. Freese, Apparent shape of super-spinning black holes, Phys. Rev. D 79 (2009) 043002, arXiv:0812.1328.

[15] C. Bambi, N. Yoshida, Shape and position of the shadow in the $\delta = 2$ Tomimatsu-Sato space-time, Class. Quantum Gravity 27 (2010) 205006, arXiv:1004.3149.

[16] R.A. Konoplya, T. Pappas, A. Zhidenko, Einstein-scalar–Gauss-Bonnet black holes: analytical approximation for the metric and applications to calculations of shadows, Phys. Rev. D 101 (2020) 044054, arXiv:1907.10112.

[17] S.-W. Wei, Y.-C. Zou, Y.-X. Liu, R.B. Mann, Curvature radius and Kerr black hole shadow, J. Cosmol. Astropart. Phys. 08 (2019) 030, arXiv:1904.07710.

[18] S.-W. Wei, Y.-X. Liu, R.B. Mann, Intrinsic curvature and topology of shadows in Kerr spacetime, Phys. Rev. D 99 (2019) 041303, arXiv:1811.00047.

[19] H.-M. Wang, Y.-M. Xu, S.-W. Wei, Shadows of Kerr-like black holes in a modified gravity theory, J. Cosmol. Astropart. Phys. 03 (2019) 046, arXiv:1810.12767.

[20] C. Liu, T. Zhu, Q. Wu, K. Jusufi, M. Jamil, M. Azreg-Aïnou, A. Wang, Shadow and quasinormal modes of a rotating loop quantum black hole, Phys. Rev. D 101 (2020) 084001, arXiv:2003.00477.

[21] R. Kumar, S.G. Ghosh, A.-Z. Wang, Shadow cast and deflection of light by charged rotating regular black holes, Phys. Rev. D 100 (2019) 124024, arXiv:1912.05154.

[22] P.V.P. Cunha, C.A.R. Herdeiro, Shadows and strong gravitational lensing: a brief review, Gen. Relativ. Gravit. 50 (2018) 42, arXiv:1801.00860.

[23] T. Ohgami, N. Sakai, Wormhole shadows, Phys. Rev. D 91 (2015) 124020, arXiv: 1704.07065.

[24] P.G. Nedkova, V.K. Tinchev, S.S. Yazadjiev, Shadow of a rotating traversable wormhole, Phys. Rev. D 88 (2013) 124019, arXiv:1307.7647.

[25] R. Shaikh, Shadows of rotating wormholes, Phys. Rev. D 98 (2018) 024044, arXiv:1803.11422.

[26] M. Amir, A. Banerjee, S.D. Maharaj, Shadow of charged wormholes in Einstein–Maxwell–dilaton theory, Ann. Phys. 400 (2019) 198, arXiv:1805.12435.

[27] M. Amir, K. Jusufi, A. Banerjee, S. Hansraj, Shadow images of Kerr-like wormholes, Class. Quantum Gravity 36 (2019) 215007, arXiv:1806.07782.

[28] X.-B. Wang, P.-C. Li, C.-Y. Zhang, M. Guo, Novel shadows from the asymmetric thin-shell wormhole, Phys. Lett. B 811 (2020) 135930, arXiv:2007.03327.

[29] Z. Chang, Q.-H. Zhu, Does the shape of the shadow of a black hole depend on motional status of an observer?, Phys. Rev. D 102 (2020) 044012, arXiv: 2006.00685.

[30] S.E. Gralla, A. Lupsasca, Observable shape of black hole photon rings, Phys. Rev. D 102 (2020) 124003, arXiv:2007.10336.

[31] Event Horizon, Telescope collaboration, first M87 event horizon telescope results. I. The shadow of the supermassive black hole, Astrophys. J. 875 (2019) L1, arXiv:1906.11238.

[32] Event Horizon Telescope collaboration, First M87 event horizon telescope results. II. Array and instrumentation, Astrophys. J. 875 (2019) L2, arXiv:1906. 11239.

[33] Event Horizon Telescope collaboration, First M87 event horizon telescope results. III. Data processing and calibration, Astrophys. J. 875 (2019) L3, arXiv: 1906.11240.

[34] Event Horizon Telescope collaboration, First M87 event horizon telescope results. IV. Imaging the central supermassive black hole, Astrophys. J. 875 (2019) L4, arXiv:1906.11241.

[35] Event Horizon Telescope collaboration, First M87 event horizon telescope results.V. Physical origin of the asymmetric ring, Astrophys. J. 875 (2019) L5, arXiv:1906.11242.

[36] Event Horizon Telescope collaboration, First M87 event horizon telescope results. VI. The shadow and mass of the central black hole, Astrophys. J. 875 (2019) L6, arXiv:1906.11243.

[37] Y. Meng, X.-M. Kuang, Z.-Y. Tang, Photon regions, shadow observables, and constraints from M87* of a charged rotating black hole, Phys. Rev. D 106 (2022) 064006, arXiv:2204.00897.

[38] X.-M. Kuang, Z.-Y. Tang, B. Wang, A.-Z. Wang, Constraining a modified gravity theory in strong gravitational lensing and black hole shadow observations, Phys. Rev. D 106 (2022) 064012, arXiv:2206.05878.

[39] S.V.M.C.B. Xavier, H.C.D.L. Junior, L.C.B. Crispino, Shadows of black holes with dark matter halo, Phys. Rev. D 107 (2023) 064040, arXiv:2303.17666.

[40] X.M. Kuang, A. Övgün, Strong gravitational lensing and shadow constraint from M87* of slowly rotating Kerr-like black hole, Ann. Phys. 447 (2022) 169147, arXiv:2205.11003.

[41] K. Destounis, A.G. Suvorov, K.D. Kokkotas, Testing spacetime symmetry through gravitational waves from extreme-mass-ratio inspirals, Phys. Rev. D 102 (2020) 064041, arXiv:2009.00028.

[42] K. Destounis, A.G. Suvorov, K.D. Kokkotas, Gravitational-wave glitches in chaotic extreme-mass-ratio inspirals, Phys. Rev. Lett. 126 (2021) 141102, arXiv:2103. 05643.

[43] K. Destounis, K.D. Kokkotas, Gravitational-wave glitches: resonant islands and frequency jumps in non-integrable extreme-mass-ratio inspirals, Phys. Rev. D 104 (2021) 064023, arXiv:2108.02782.

[44] K. Destounis, G. Huez, K.D. Kokkotas, Geodesics and gravitational waves in chaotic extreme-mass-ratio inspirals: the curious case of Zipoy-Voorhees black-hole mimickers, Gen. Relativ. Gravit. 55 (2023) 71, arXiv:2301.11483.

[45] E. Maggio, M. van de Meent, P. Pani, Extreme mass-ratio inspirals around a spinning horizonless compact object, Phys. Rev. D 104 (2021) 104026, arXiv: 2106.07195.

[46] K. Destounis, F. Angeloni, M. Vaglio, P. Pani, Extreme-mass-ratio inspirals into rotating boson stars: nonintegrability, chaos, and transient resonances, arXiv: 2305.05691.

[47] V. Cardoso, K. Destounis, F. Duque, R.P. Macedo, A. Maselli, Black holes in galaxies: environmental impact on gravitational-wave generation and propagation, Phys. Rev. D 105 (2022) L061501, arXiv:2109.00005.

[48] V. Cardoso, K. Destounis, F. Duque, R.P. Macedo, A. Maselli, Gravitational waves from extreme-mass-ratio systems in astrophysical environments, Phys. Rev. Lett. 129 (2022) 241103, arXiv:2210.01133.

[49] K. Destounis, A. Kulathingal, K.D. Kokkotas, G.O. Papadopoulos, Gravitational-wave imprints of compact and galactic-scale environments in extreme-mass-ratio binaries, Phys. Rev. D 107 (2023) 084027, arXiv:2210.09357.

[50] E. Figueiredo, A. Maselli, V. Cardoso, Black holes surrounded by generic dark matter profiles: appearance and gravitational-wave emission, Phys. Rev. D 107 (2023) 104033, arXiv:2303.08183.

[51] H. Weyl, Zur Gravitationstheorie, Ann. Phys. (Berlin) 359 (1917) 117.

[52] E. Newman, L. Tamburino, New approach to Einstein's empty space field equations, J. Math. Phys. (N. Y.) 2 (1961) 667.

[53] I. Robinson, Some spherical gravitational waves in general relativity, Proc. R. Soc. A 265 (1962) 463.

[54] J.B. Griffiths, P. Krtous, J. Podolsky, Interpreting the C-metric, Class. Quantum Gravity 23 (2006) 6745.

[55] W. Kinnersley, M. Walker, Uniformly accelerating charged mass in general relativity, Phys. Rev. D 2 (1970) 1359.

[56] J. Plebański, M. Demiański, Rotating, charged, and uniformly accelerating mass in General Relativity, Ann. Phys. 98 (1976) 98.

[57] J.B. Griffiths, J. Podolsky, A new look at the Plebanski-Demianski family of solutions, Int. J. Mod. Phys. D 15 (2006) 335, arXiv:gr-qc/0511091.

[58] M. Appels, R. Gregory, D. Kubizňák, Thermodynamics of accelerating black holes, Phys. Rev. Lett. 117 (2016) 131303, arXiv:1604.08812.

[59] M. Appels, R. Gregory, D. Kubizňák, Black hole thermodynamics with conical defects, J. High Energy Phys. 1705 (2017) 116, arXiv:1702.00490.

[60] M. Astorino, Thermodynamics of regular accelerating black holes, Phys. Lett. B 760 (2016) 393, arXiv:1612.04387.

[61] R. Gregory, Accelerating black holes, J. Phys. Conf. Ser. 942 (2017) 012002, arXiv:1712.04992.

[62] K. Destounis, R.D.B. Fontana, F.C. Mena, Accelerating black holes: quasinormal modes and late-time tails, Phys. Rev. D 102 (2020) 044005, arXiv:2005.03028.

[63] K. Destounis, R.D.B. Fontana, F.C. Mena, Stability of the Cauchy horizon in accelerating black-hole spacetimes, Phys. Rev. D 102 (2020) 104037, arXiv: 2006.01152.

[64] K. Destounis, G. Mascher, K.D. Kokkotas, Dynamical behavior of the C-metric: charged scalar fields, quasinormal modes and superradiance, Phys. Rev. D 105 (2022) 124058, arXiv:2206.07794.

[65] R.D.B. Fontana, F.C. Mena, Quasinormal modes and stability of boosted RN AdS black holes, J. High Energy Phys. 2210 (2022) 047, arXiv:2203.13933.

[66] A. Grenzebach, V. Perlick, C. Lämmerzahl, Photon regions and shadows of accelerated black holes, Int. J. Mod. Phys. D 24 (2015) 1542024, arXiv:1503.03036.

[67] M. Zhang, J. Jiang, Shadows of accelerating black holes, Phys. Rev. D 103 (2021) 025005, arXiv:2010.12194.

[68] A. Anabalón, F. Gray, R. Gregory, D. Kubizňák, R.B. Mann, Thermodynamics of charged, rotating, and accelerating black holes, J. High Energy Phys. 04 (2019) 096, arXiv:1811.04936.

[69] B. Carter, Global structure of the Kerr family of gravitational fields, Phys. Rev. 174 (1968) 1559.

[70] P.V.P. Cunha, C.A.R. Herdeiro, E. Radu, H.F. Runarsson, Shadows of Kerr black holes with and without scalar hair, Int. J. Mod. Phys. D 25 (2016) 1641021, arXiv:1605.08293.

[71] V. Perlick, O.Y. Tsupko, Calculating black hole shadows: review of analytical studies, Phys. Rep. 947 (2022) 1, arXiv:2105.07101.

[72] A. Grenzebach, V. Perlick, C. Lämmerzahl, Photon regions and shadows of Kerr-Newman-NUT black holes with a cosmological constant, Phys. Rev. D 89 (2014) 124004, arXiv:1403.5234.

[73] N. Tsukamoto, Black hole shadow in an asymptotically-flat, stationary, and axisymmetric spacetime: the Kerr-Newman and rotating regular black holes, Phys. Rev. D 97 (2018) 064021, arXiv:1708.07427.

[74] S.V.M.C.B. Xavier, P.V.P. Cunha, L.C.B. Crispino, C.A.R. Herdeiro, Shadows of charged rotating black holes: Kerr–Newman versus Kerr–Sen, Int. J. Mod. Phys. D 29 (2020) 2041005, arXiv:2003.14349.

[75] K. Hioki, K.-i. Maeda, Measurement of the Kerr spin parameter by observation of a compact object's shadow, Phys. Rev. D 80 (2009) 024042, arXiv:0904.3575.

[76] D. Psaltis, L. Medeiros, P. Christian, F. Ozel, the EHT Collaboration, Gravitational test beyond the first post-Newtonian order with the shadow of the M87 black hole, Phys. Rev. Lett. 125 (2020) 141104, arXiv:2010.01055.

[77] P. Kocherlakota, et al., Event Horizon Telescope, Constraints on black-hole charges with the 2017 EHT observations of M87*, Phys. Rev. D 103 (2021) 104047, arXiv:2105.09343, arXiv:2105.09343.

[78] M. Afrin, R. Kumar, S.G. Ghosh, Parameter estimation of hairy Kerr black holes from its shadow and constraints from M87*, Mon. Not. R. Astron. Soc. 504 (2021) 5927, arXiv:2103.11417.

[79] C. Bambi, K. Freese, S. Vagnozzi, L. Visinelli, Testing the rotational nature of the supermassive object M87* from the circularity and size of its first image, Phys. Rev. D 100 (2019) 044057, arXiv:1904.12983.

[80] M. Afrin, S.G. Ghosh, Constraining rotating black holes in Horndeski theory with EHT observations of M87*, Astrophys. J. 932 (2022) 51, arXiv:2110.05258.

[81] R. Kumar, S.G. Ghosh, Black hole parameter estimation from its shadow, Astrophys. J. 892 (2020) 78, arXiv:1811.01260.

[82] I. Banerjee, S. Chakraborty, S. SenGupta, Constraining a modified gravity theory in strong gravitational lensing and black hole shadow observations, Phys. Rev. D 101 (2020) 041301, arXiv:1909.09385.

[83] A.A. Abdujabbarov, L. Rezzolla, B.J. Ahmedov, A coordinate-independent characterization of a black hole shadow, Mon. Not. R. Astron. Soc. 454 (2015) 2423, arXiv:1503.09054.